



## Structural complexity resulting from pervasive ductile deformation in the Karakoram Shear Zone, Ladakh, NW India

M. R. McCarthy<sup>1</sup> and R. F. Weinberg<sup>1</sup>

Received 21 July 2008; revised 5 October 2009; accepted 23 November 2009; published 19 May 2010.

[1] The NW-SE trending, ~800 km long, dextral Karakoram Shear Zone bounds southwest Tibet. We investigate an area immediately NW of the Pangong Lake where midcrustal rocks sections of the shear zone are exposed. Here, the dominant shear zone is characterized by dextral mylonitic rocks sheared at amphibolite facies and partly retrogressed to greenschist facies. These rocks define a kilometric, SE plunging inclined-to-recumbent fold in the footwall of a north directed, oblique dextral thrust that exhumed anatexitic rocks of the Pangong Range. Argon cooling ages reveal that the Pangong Range cooled from ~700°C to 300°C between ~18–15 and ~10 Ma, contemporaneously with overthrusting. Toward the SE, closer to the Pangong Lake, this kilometric fold is rotated from its NW–SE trend to an E–W trend, and the sense of shear changes to sinistral, with a broadly north directed thrusting component. The documented structures contradict predictions of normal movement in this area derived from considerations of rigid block behavior of the crust and support the interpretation that the system records dextral transpression. Thrusting and exhumation of the deeper and hot rocks exposed in the Pangong Range, folding of the thrust footwall, and the development of a sinistral E–W trending shear zone are all compatible with transpression caused by a northward push by a rigid indenter such as the Ladakh Batholith. **Citation:** McCarthy, M. R., and R. F. Weinberg (2010), Structural complexity resulting from pervasive ductile deformation in the Karakoram Shear Zone, Ladakh, NW India, *Tectonics*, 29, TC3004, doi:10.1029/2008TC002354.

### 1. Introduction

[2] The Karakoram Shear Zone is a ~800 km long, dextral strike-slip fault bounding the southwestern margin of Tibet (Figure 1). Various aspects of the Karakoram Shear Zone including age of initiation, slip rates, and finite geological offsets remain controversial. Interpretations vary greatly depending on correlation of offset geological features across the shear zone and their age, as well as the age of the shear zone [Lacassin *et al.*, 2004a; Peltzer and Tapponnier, 1988;

Rolland *et al.*, 2009; Searle, 1996; Searle *et al.*, 1998; Searle and Phillips, 2004; Upadhyay *et al.*, 2005; Valli *et al.*, 2007, 2008; Weinberg and Dunlap, 2000]. Total movement on the fault has been estimated variously to be between 40 and 150 km [Searle and Phillips, 2007], a minimum of 250 km [Lacassin *et al.*, 2004a, 2004b; Valli *et al.*, 2008], or around 300 km either on the Karakoram Fault itself [Rolland *et al.*, 2009] or distributed over a wide zone of deformation [Weinberg and Dunlap, 2000]. Estimates of the age of initiation of the shear zone also vary from 23 Ma (possibly as old as 34 Ma) [Lacassin *et al.*, 2004a; Valli *et al.*, 2007, 2008; Weinberg and Dunlap, 2000] to  $18 \pm 0.6$  Ma [Searle *et al.*, 1998] or as young as 15.7 Ma [Phillips *et al.*, 2004; Phillips and Searle, 2007] or  $13.9 \pm 0.1$  Ma [Bhutani *et al.*, 2003]. Correspondingly, calculated slip rates range from around 3–5 mm/yr [Brown *et al.*, 2002; Wright *et al.*, 2004] to 10 mm/yr [Chevalier *et al.*, 2005; Lacassin *et al.*, 2004a].

[3] A number of studies have focused on the structural and metamorphic characterization of the shear zone [Lacassin *et al.*, 2004a; Murphy *et al.*, 2000, 2002; Murphy and Burgess, 2006; Phillips and Searle, 2007; Ravikant, 2006; Rolland and Pécher, 2001; Rolland *et al.*, 2009; Rutter *et al.*, 2007; Valli *et al.*, 2007, 2008; Weinberg *et al.*, 2000], but information regarding the temporal and spatial structural evolution is lacking over large portions of the shear zone. On the basis of remote sensing studies, Raterman *et al.* [2007] defined a triple junction in a remote and currently inaccessible part of Karakoram mountains in Ladakh. In this area, the dextral Karakoram Shear Zone is interpreted to intersect the sinistral, E–W trending, Longmu Tso Fault (Figure 1). This fault is part of a system of faults that link up with the sinistral Altyn Tagh Fault, another major transcurrent fault bounding the Tibetan Plateau. Raterman *et al.* defined a 27 km wide bend of the Karakoram Shear Zone (Figure 2), where it curves around the NE margin of Pangong Range, and ascribed the bend to contemporaneous sinistral motion on the Longmu Tso Fault, which would impose transtension south of the junction. Using a rigid block conceptualization of continental crust deformation and using estimates for current movement rates on the fault system, they carried out kinematic analysis which supported transtension in the area of the Pangong Range, south of the bend, and allowed for an estimate of the rate of lateral movement that created the bend. This interpretation contrasts with the structural study of Weinberg *et al.* [2000], who interpreted the Pangong Range as an exhumed pop-up block of migmatites resulting from transpression between two strands of the Karakoram Shear Zone: the NE Pangong Strand and the SW Tangtse Strand (Figure 2). They found no evidence for transtension in the area.

<sup>1</sup>School of Geosciences, Monash University, Clayton, Victoria, Australia.

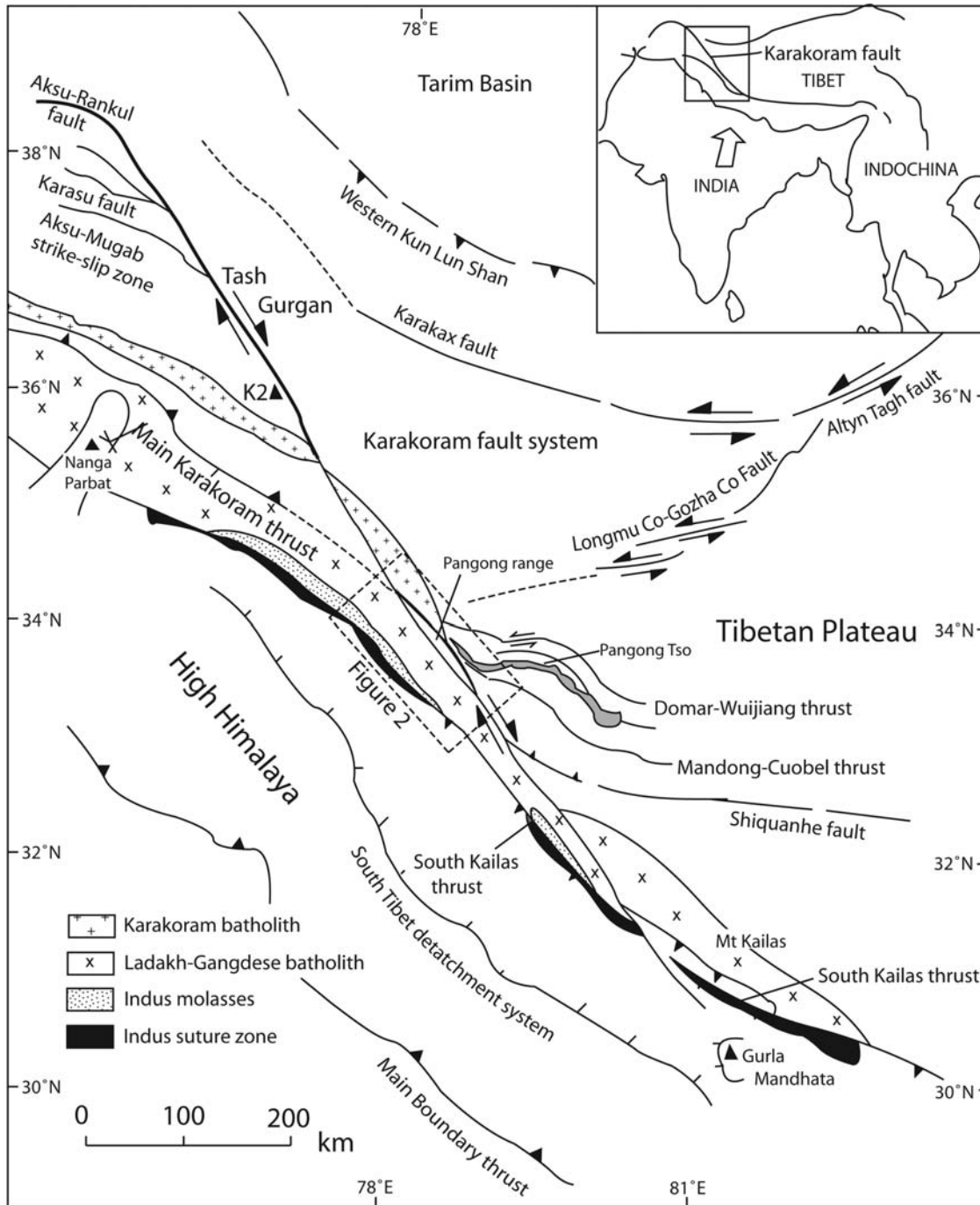


**Figure 1.** Map of the Karakoram fault system, showing adjacent major structures in western Himalayas. Modified from *Searle et al.* [1998].

[4] Understanding the nature of deformation in this region where the Karakoram Shear Zone links up with the sinistral system that ultimately focus into the Alтын Tagh Fault (Figure 1) may help us to better constrain the balance between pervasive deformation and rigid block translation during continental collision. In this paper we investigate the structural and metamorphic evolution of a triple junction in the Pangong Tso (Pangong lake). This junction is 40 km

south of and similar to that defined by *Rateman et al.* [2007]. In the Pangong Tso area, the NE Pangong Strand of the Karakoram Shear Zone intersects the newly defined E-W trending sinistral Phobrang Shear Zone (Figure 2).

[5] This paper starts with a brief section on methodology, followed by a description of the deformation related to the Karakoram Shear Zone, away from this newly defined triple junction. Here, a kilometeric-scale fold of mylonitic rocks

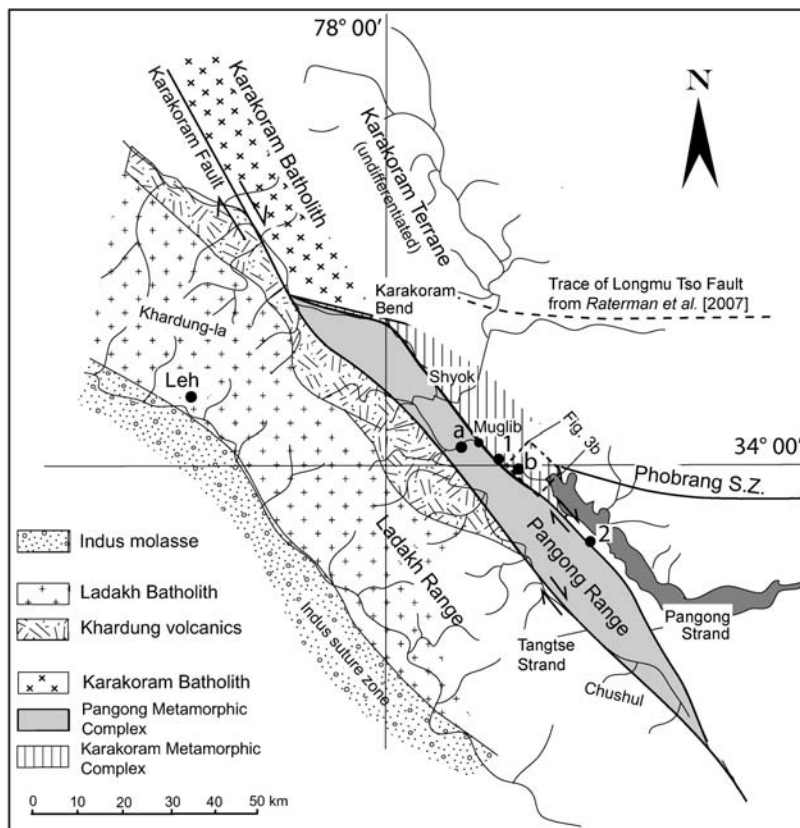


**Figure 2.** Simplified regional geological map of the Karakoram Fault in northern Ladakh, showing the Pangong Range bounded by the Pangong and Tangtse strands. Position of Longmu Tso is from *Raterman et al.* [2007]. Points 1 and 2 correspond to fault scarps indicating Quaternary movement on Pangong Strand from *Brown et al.* [2002]. Locations for samples used for  $^{40}\text{Ar}/^{39}\text{Ar}$  dating are TNG45mm (point a) and PNG19 (point b). SZ, shear zone.

resulted from oblique dextral thrusting of the Pangong Range over rocks of the Karakoram Metamorphic Complex. We then proceed to describe the nature of deformation in the Phobrang Shear Zone and relationships where the two meet. We end by speculating about the origin and broader role of the triple junction in the context of eastern Ladakh.

## 2. Methodology

[6] A detailed geological and structural field study was undertaken in order to establish movement history on the Karakoram Shear Zone in the Pangong Tso region. Field work was limited by a combination of mountainous topography and accessibility to this sensitive border region between India and Tibet. The majority of localities documented had clear indicators of shear sense and in any one locality, we used several observations of at least two different types of kinematic indicators to determine shear sense. Field mapping and interpretation of satellite images was accompanied by structural analyses and petrographic studies.

[7] The  $^{40}\text{Ar}/^{39}\text{Ar}$  cooling age determinations of two samples were carried out. Hornblende and biotite were extracted by crushing the samples using standard methods

before magnetic separation and tapping on a sheet of paper. Approximately 50 mg of each mineral with a minimum grain size of 0.3–0.1 mm were separated. The samples were then irradiated in position 5c at the McMaster reactor, Hamilton, Ontario, Canada.

[8] The  $^{40}\text{Ar}/^{39}\text{Ar}$  isotope analyses were performed at the Noble Gas Geochronology and Geochemistry laboratory, the University of Melbourne. Analytical procedures were analogous to those described by *Phillips et al.* [2007] and *Phillips and Harris* [2008]. Step-heating analyses of biotite (TNG45) and hornblende (TNG19) samples were carried out using a tantalum furnace connected to a VG3600 mass spectrometer equipped with a Daly detector. Laser step-heating analyses were also conducted on hornblende from sample TNG45, which had insufficient mass for furnace step heating, using a Spectron Nd-YAG laser connected to a Micromass 5400 mass spectrometer with a Daly detector. The neutron fluence monitor used was GA1550 biotite ( $98.8 \pm 0.5$  Ma) [*Renne et al.*, 1998], which yielded J values ranging from  $0.004786 \pm 0.000018$  (0.38%,  $2\sigma$ ) to  $0.004789 \pm 0.000016$  (0.33%,  $2\sigma$ ). Mass discrimination was monitored by measuring air aliquots from calibrated pipette systems. Correction factors for interfering isotopes were



**Figure 3a.** ASTER image of the Pangong Tso region in eastern Ladakh with locality names, major geological features, and summary of structural information. Key localities are Chagar Tso (lake in the center of the image), Pangong Tso in the lower right, Karakoram Range to the north, and Pangong Range to the south of the Muglib Valley. The thick black line marks the approximate position of the plane separating the Karakoram and Pangong metamorphic complexes (MC) inferred from the image combined with field observations. Note that the dip of this contact changes from vertical in the NW to 45° SW in the central part of the image. Rocks on either side are strongly sheared and compose the Karakoram Shear Zone. The northeastern limit of the shear zone remains unknown. Structural symbols summarize information for different areas, arrows represent lineations, and arrow head indicates the motion direction of hanging wall, parallel to lineation (full data are in stereonet in Figure 3b). Notice that in the Pangong Range rocks dip 45° SW, whereas in the upper reaches of the Karakoram Range, they dip 60° NE. The locations of Figures 6a–6d, 8, 9, and 10 are indicated, and small arrows mark viewing direction. Shearing along the main valley and to the north is dominantly dextral strike slip; shearing determined in the small SW trending valley, SSW of Chagar Tso, into the Pangong Range marked by a thick dashed line, revealed a significant thrusting component of motion (see Figure 9). Close to Pangong Tso, shearing is dominantly sinistral strike slip. Lines indicating folding and faulting in the NE corner of the image are interpreted from image only.

$(^{39}\text{Ar}/^{37}\text{Ar})_{\text{Ca}} = 6.80 (\pm 0.05) \times 10^{-4}$ ;  $(^{36}\text{Ar}/^{37}\text{Ar})_{\text{Ca}} = 2.89 (\pm 0.19) \times 10^{-4}$  and  $(^{40}\text{Ar}/^{39}\text{Ar})_{\text{K}} = 4.0 (\pm 4.0) \times 10^{-4}$ . Age plateaus are defined as including  $\geq 50\%$  of  $^{39}\text{Ar}$ , distributed over a minimum of 3 consecutive steps and coincident at the 95% confidence level.

### 3. Geological Setting

#### 3.1. Regional Geology

[9] The Karakoram Shear Zone extends along the southwestern margin of Tibet from its northern termination at the transtensional Muji basin in the central Pamir region, to the southern termination in the Mount Kailas region [Murphy *et al.*, 2002] (Figure 1). The central segment of the fault is characterized by transpressional ranges such as the Pangong Range and K2-Gasherbrum Range [Searle *et al.*, 1998], where deeper crustal rocks have been exhumed.

[10] In Ladakh, the Pangong Range is bounded by the active northeastern Pangong Strand of the Karakoram Shear

Zone and the inactive southwestern Tangtse Strand [Searle *et al.*, 1998] (Figure 2). This range is a 100 km long, ~10 km wide massif composed of the Pangong Metamorphic Complex (PMC). The range is an obliquely exhumed midcrustal section, forming a pop-up structure where hotter and deeper rocks have been exhumed in relation to colder surroundings. Exhumation is interpreted to result from dextral transpression along the Karakoram Shear Zone [Rolland and Pêcher, 2001; Rolland *et al.*, 2009; Weinberg and Mark, 2008; Weinberg *et al.*, 2000]. This interpretation is based on (1) the relative uplift of the hotter rocks of the Pangong Range in relation to the surroundings, (2) the development of upright folds trending in an orientation 10°–20° anticlockwise from contemporaneous dextral shear zones [Weinberg and Mark, 2008], and (3) regions characterized by inclined lineations in mylonites indicating a thrusting component [Weinberg *et al.*, 2000].

[11] The PMC is composed predominantly of migmatitic granitoids, migmatitic biotite-amphibolites to gneisses, bio-

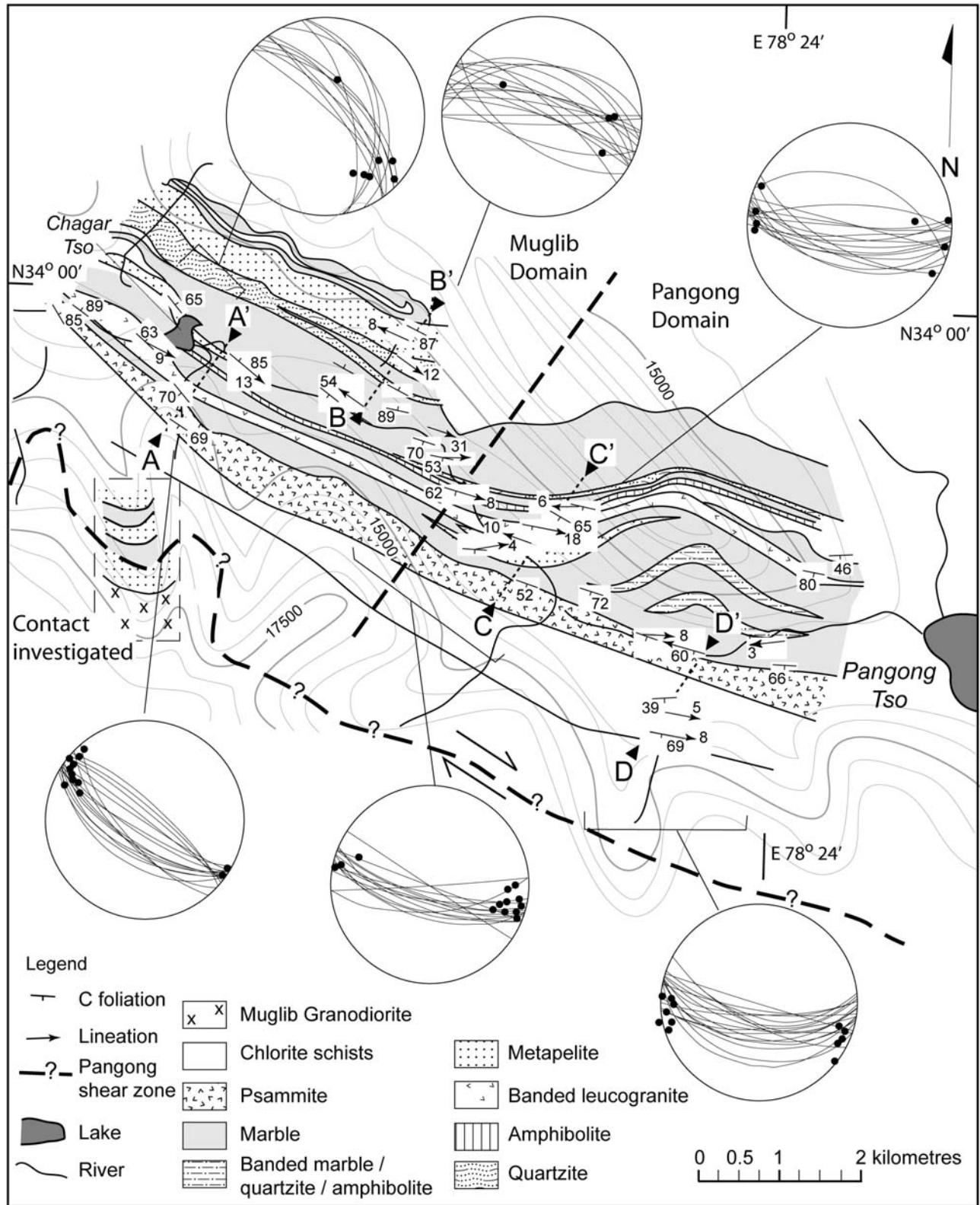
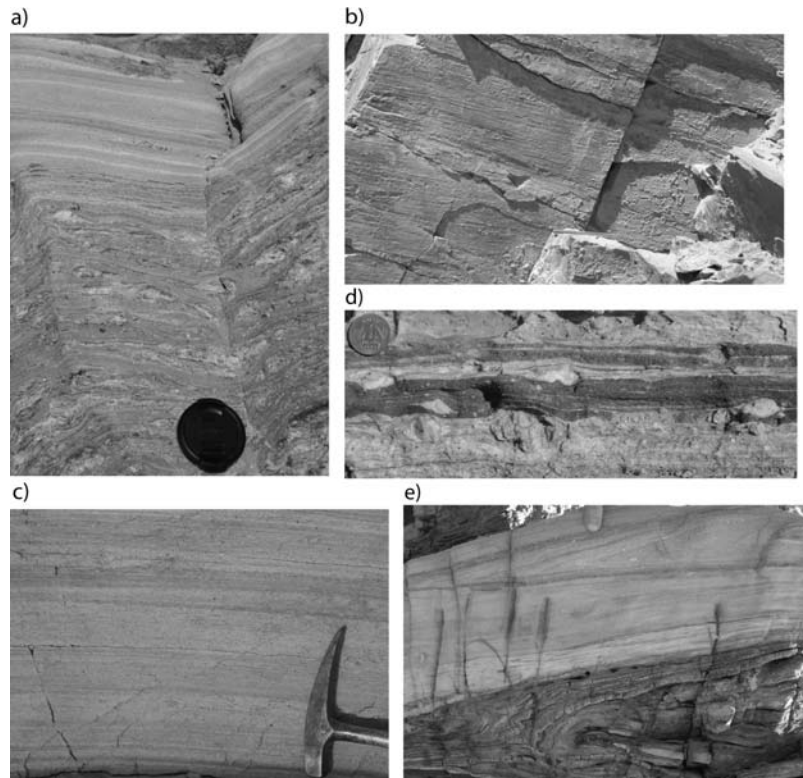


Figure 3b



**Figure 4.** (a) Banded sheared marble. More competent, quartz-rich bands deformed into asymmetric lenses by dextral shearing. (b) Steep wall parallel to layering in marble showing the strong pervasive lineation that characterizes nearly all rock types in the area. Lineation plunging gently to the SE; pen for scale is nearly horizontal. (c) Leucogranite mylonite. (d) Pegmatitic leucogranite and mafic band with K-feldspar porphyroclasts, outcrop surface perpendicular to foliation parallel to lineation. (e) Shear fold in leucogranite mylonite in contact with amphibolite mylonite, looking down plunge of the lineation. All photographs are from outcrops immediately NW of Chagar Tso.

tite schists and psammities, calc-silicate rocks and leucogranite intrusions [Weinberg and Mark, 2008]. Leucogranites in the Pangong Range have been dated to between 20 and 15 Ma [e.g., Reichardt *et al.*, 2010; Searle *et al.*, 1998]. The Ladakh terrane lies to the southwest of the Karakoram Shear Zone and consists predominantly of precollisional calc-alkaline rocks forming the Ladakh Batholith, and the associated Khardung volcanic rocks (Figure 2), which were a part of the Cretaceous Kohistan-Ladakh island arc [Weinberg and Dunlap, 2000]. Step heating Ar isotope experiments in K-feldspar from a sample collected in the vicinity of the Karakoram Shear Zone in Ladakh indicates that at least parts of the batholith have remained at temperatures below

150°C since 36 Ma, that is, since before anatexis in the Karakoram Shear Zone [Dunlap *et al.*, 1998].

[12] The Karakoram terrane is located northeast of the Karakoram Shear Zone and consists in this area of Paleozoic-Mesozoic sedimentary rocks of the Asian plate known as the Karakoram Metamorphic Complex (KMC). We follow the literature and ascribe to the KMC a package of rocks composed predominantly of garnet-biotite-staurolite schists, marbles, amphibolites, calc-schists, and quartzo-feldspathic mica schists grading to psammities [Dunlap *et al.*, 1998], including a bedding-parallel leucogranite sheet, modally and texturally similar to those that form the bulk of the Karakoram Batholith in Ladakh [Weinberg and Mark, 2008].

**Figure 3b.** Geological and structural map, showing two structural domains separated by the bold, NW–SE trending dashed line. The northern Karakoram Shear Zone (or Muglib) domain is characterized by dextral shearing on a NW–SE trending fabric. In the southern Phobrang Shear Zone (or Pangong) domain the fabric rotates to close to E–W. Equal-area, lower hemisphere stereographic projections of C planes and lineations for different areas. A–A', B–B', C–C', D–D' mark the position of cross sections used to construct Figure 7. Widespread and well-defined dextral shear indicators characterize the northern Muglib domain, whereas sinistral shear indicators characterize the southern Pangong domain (shear senses not marked on map). A zone of ambiguous or coexisting sinistral and dextral indicators define a transition zone between the two domains. Dashed box on west side marks region between Karakoram Metamorphic Complex, characterized by interlayered marble and metapelites, and Pangong Metamorphic Complex, characterized by anatexitic schists in contact with Muglib Batholith.



**Figure 5.** Interlayered, gradational contact between sheared amphibolite (dark unit, left) and marble (right; 33° 58'36.2"N, 78°22'37.5"E).

The KMC differs from the PMC by the presence of thick layers of marble and rarity of leucogranites. Also, KMC rocks underwent only lower amphibolite to greenschist facies metamorphism and therefore lack migmatites.

### 3.2. Geology of the Muglib Valley in the Pangong Tso Region

[13] The Muglib Valley, along the NE side of the Pangong Range, trends northwest-southeast for ~30 km (Figure 2) from the northern tip of the Pangong Tso, a drowned river valley dammed by tectonic uplift at its northwestern end as a result of recent movement on the Pangong Strand [Searle *et al.*, 1998]. We focus on a region immediately northwest of the lake (Figures 3a and 3b), where rocks exposed in the valley and to the north are part of the Karakoram Metamorphic Complex and consist predominantly of recrystallized massive marble units, pelitic and psammitic schists, quartzites and amphibolites, with many of the lithologies showing extensive interlayering, likely to be a combined result of primary bedding and shearing. The sequence is strongly sheared into protomylonites to mylonites with well-developed mineral and stretching lineations [see also Rolland *et al.*, 2009].

[14] The marble units, which stand out in the sequence, form layers up to ~700 m thick, range from a creamy sandy-pink to dark blue-gray quartz-rich beds, medium-coarse grained, mostly massive but with faint banding parallel to contacts apparent in some areas, possibly representing relict bedding. In the darker, brown, contaminated marbles and blue-gray quartz-rich marbles, shearing is defined by deformation of more competent bands (Figure 4a). In the massive marbles, the mylonitic fabric is represented by well-defined color banding and strong stretching lineation (Figure 4b), with rare intrafolial isoclinal folds parallel to regional fabric.

[15] The most distinctive unit in the sequence is a single band of mylonitic leucogranite up to 200 m wide in places and parallel to bedding (Figures 4c–4e). The presence of feldspar porphyroclasts up to 2 cm in size in a finer grained matrix of quartz, feldspar, muscovite and biotite ± garnet suggests it was a pegmatitic leucogranite. It is interlayered with bands and pods of amphibolite, typically <1 m thick (Figure 4c).

[16] There are a number of banded units up to tens of meters thick, within and between the massive marble beds (Figures 3a and 3b). These consist of interlayered marble ± amphibolite ± schists (Figure 5), with both continuous and lenticular bands ranging in width from <20 cm to 1 m. The amphibolite units, present as a continuous band up to 60 m thick, as well as thin layers in banded sequences, are fine-grained consisting predominantly of hornblende, biotite, plagioclase, minor quartz, and garnet, retrogressed in the southern part of the valley to tremolite-actinolite + chlorite + calcite representing a greenschist facies paragenesis.

[17] There are a number of biotite schist layers in the area, ranging in composition from quartz and feldspar-rich psammitic schists, to muscovite and biotite-rich schists including garnet in places, and minor sillimanite [Rolland *et al.*, 2009]. These layers range in thickness from tens of meters up to 300–400 m thick. Chlorite schists in Figures 3a and 3b represent a greenschist facies retrogression of the amphibolite facies assemblages and dominate the south and southwestern part of the valley (Figures 3a and 3b). Retrogression is gradational, first appearing as narrow bands of chlorite schist surrounding quartz veins in amphibolites. Retrogression increases in intensity southward into the Pangong Range, where the alteration is pervasive, represented by chlorite-actinolite-calcite schists with euhedral pyrite and magnetite grains up to 1 cm in size.

## 4. Structural Geology

### 4.1. General Features

[18] Although our focus is the dominant ductile deformation there is evidence for local brittle deformation [e.g., Rutter *et al.*, 2007], such as brecciation of the marble southeast of Chagar Tso or Chagar lake (Figures 3a and 3b). This brecciated unit is ~40 m thick, with clasts ranging from large subrounded blocks to smaller, angular blocks with jigsaw fit in fine-grained calcite cement. Fault planes with brecciated marble were documented throughout the field area, commonly trending NNE–SSW parallel to some of the deeper valleys in the ranges. Within the same marble unit, ~4 km ESE of “a” in Figure 2, the marble exposed in a road cut is faulted and folded (“b” in Figure 2). The fault, traceable for ~30 m, dips moderately toward the SSW, thrusting large open folds over tight asymmetric folds plunging shallowly ~WNW. Generally, however, detailed mapping revealed that the extent of brittle deformation in the area is limited, with layers preserving continuity across the map (Figure 3b).

[19] Rocks in the region have undergone intense ductile deformation, with the pervasive regional shear plane (C plane) subparallel to bedding and to the main trend of the Karakoram Shear Zone. The intensity of deformation varies

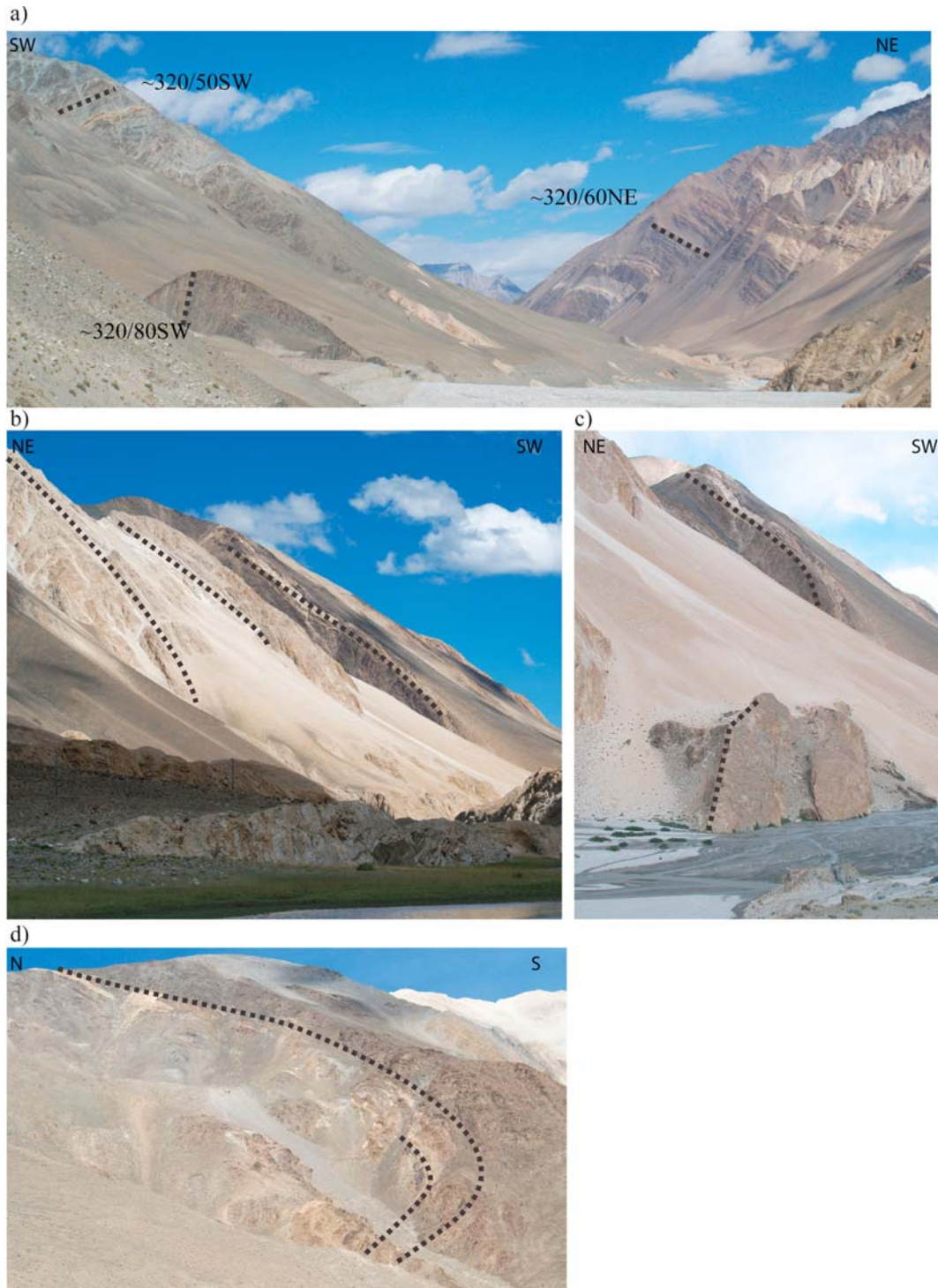


**Figure 6.** Views from the Muglib Valley at ~4200 m. See Figure 3a for approximate location. (a) Looking NW. Foliation parallel to bedding dips moderately to SW in the Pangong Range (left) and moderately NE in the Karakoram Range (right). Notice three marble bands in the Karakoram Range; the base of the highest band is at ~4900 m. In the valley, foliation is dominantly steep to subvertical. Foliation/bedding defines a large-scale fold visible looking SE from the same location. (b) Large-scale open fold hinge of the Karakoram Metamorphic Complex in the Karakoram Range (vertical scale is ~1 km). (c) Another view of fold in Figure 6b, from farther south. Note that the upper limb of this large fold (Figures 6b and 6c) dips to the SW and the lower limb to the NE. (d) The core of an inclined fold in marble of the Karakoram Range.

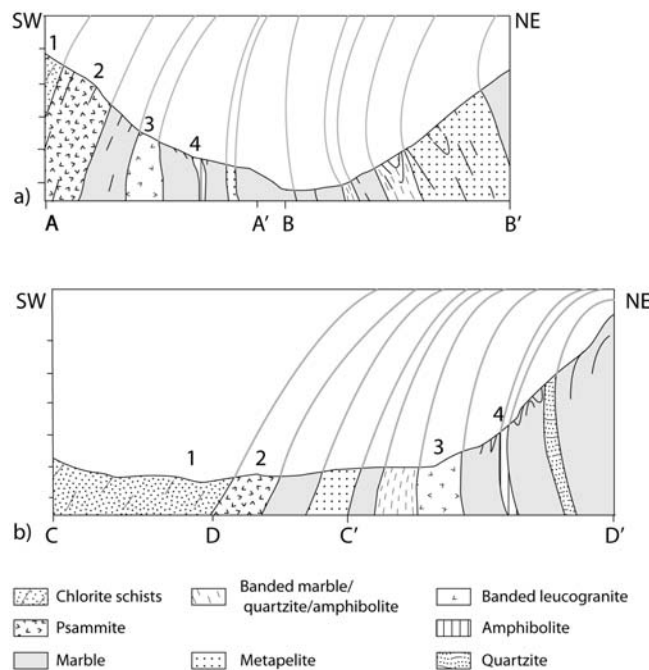


**Figure 7.** Combined cross sections based on the four cross sections (A-A', B-B', C-C', D-D') marked in Figure 3, depicting changes in dip defining a large, inclined fold. Lines above the surface are contacts projected from along strike. (a) Cross section of the northern part of Figure 3, across the area in Figure 6a. (b) Cross section of the southern part of Figure 3, across the area in Figure 6b. Cross sections focus on the lower reaches of the mountain sides depicted in Figure 6 and therefore do not include the gentler dips at high altitude. Numbers 1 to 4 link layers that appear in both profiles and reveal that the rock package thickens to the south. The northern area (Figure 7a) comprises the lower limb of the fold, whereas the southern area (Figure 7b) comprises the hinge and part of the upper limb, suggesting that the regional plunge of the fold is gently SE.

with rock type. For example, more competent amphibolite layers are boudinaged within pegmatitic leucogranite mylonite. A number of textures document shear intensity and shear sense. These include quartz ribbons and common quartz delta clasts, feldspar and sometimes garnet porphyroclasts with stair-stepping tails, C-S-C' fabric, asymmetric and intrafolial isoclinal folds, and small local sheath folds. Most rocks in the area have a strong stretching lineation, similar in appearance to striations (Figure 4a), commonly visible from meters away. Lineations are also defined by the alignment of elongated minerals such as amphiboles, as well as quartz ribbons and aggregates of mica or amphibole.

[20] In order to further detail the structural evolution, we divide the area into two structural domains (Figures 3a and 3b). The Karakoram Shear Zone domain, to the north, away from the influence of the triple junction, and the Phobrang Shear Zone domain, to the south, characterized by sinistral shearing and including a transitional zone characterized by both sinistral and dextral shearing.

#### 4.2. Karakoram Shear Zone Domain

[21] This domain extends from NW of the Chagar Tso to ~6 km northwest of the Pangong Tso (Figure 3b). In nature, it continues NW way beyond the limits of Figure 3b. This domain has unit contacts trending subparallel to the regional pervasive dextral mylonitic fabric with an average strike of 120°–140°, roughly parallel to the main trend of the valley and the Karakoram Shear Zone. Changes in dips define a kilometer-scale, inclined-to-recumbent fold visible in vertical cross sections (Figures 6 and 7), plunging moderately shallowly toward the SE. Isoclinal folds were documented on the Karakoram Range, on the northern side of the valley.

[22] Mineral and stretching lineations generally plunge shallowly ~0–30°, either NW or SE (Figure 8a). Two lineations can be seen on the same outcrops in many instances. These are similar in appearance and defined by similar minerals/mineral aggregates, but overprinting relationships could not be resolved. This contrasts with lineations farther north (outside the area covered here) where greenschist facies lineations plunge to the southeast, whereas amphibolite facies lineations plunge to the northwest [Weinberg *et al.*, 2009]. A crenulation lineation was also observed in a few localities, predominantly in mica-rich layers and chlorite schists. It generally plunges 25°–55° SE, parallel to local minor fold axes. This domain is characterized by dextral shearing, as indicated by C-S-C' fabrics, mineral fish, and asymmetric porphyroclasts and some small asymmetric folds.

[23] Into the Pangong Range, up along an incising valley southwest of Chagar Tso (marked in Figure 3a), crenulation lineation and fold axes of small asymmetric folds are at high angles to the stretching lineation (Figure 8b). Here, shear planes are the dominant planar anisotropy, and evidence such as C-S fabric, stair-stepping tails around feldspar porphyroblasts, and the asymmetry of foliation around deformed quartz veins, indicate transport direction parallel to the stretching lineation. Thus, deformation combines a component of dextral shearing with a component of thrusting toward the NNW (Figure 9).

#### 4.3. Phobrang Shear Zone Domain

[24] This domain is in the vicinity of the Pangong Tso, in the southern part of Figure 3b. Here, the large-scale, inclined-to-recumbent fold of the Karakoram Shear Zone domain is gently bent away from its regional fabric trending 120–140° to a more easterly trend of ~100°, defining the Phobrang Shear Zone domain. Lineations here are close to subhorizontal (stereonet in Figure 3b) and shear sense is sinistral, as indicated by C-S fabric and asymmetric folds (Figures 10a and 10b). Large-scale asymmetry of lozenges of amphibolite in marble (Figure 10c) indicates that sinistral shearing must have been accompanied (or possibly predated) by a thrusting component.

[25] In between the two domains, there is a transition zone characterized by outcrops with ambiguous shear sense or with both sinistral and dextral kinematic indicators. The leucogranite unit in Figure 3b has alternating bands up to ~20 cm thick of dextral and sinistral C-S-C' fabrics and

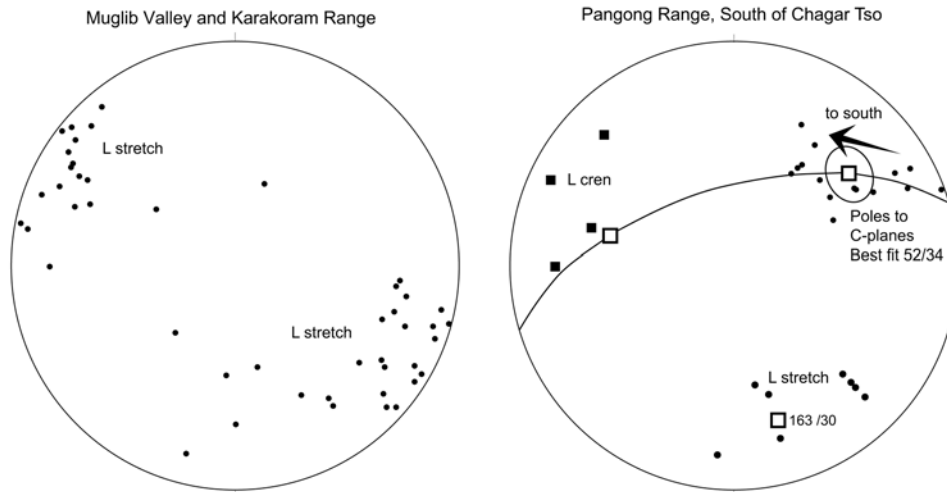


**Figure 8.** Equal-area, lower hemisphere stereographic projection of (a) stretching lineations from the Karakoram Shear Zone domain and (b) structural elements in valley into the Pangong Range southwest of Chagar Tso (Figure 3). C planes and lithological contacts become more gently dipping to the south (arrow), reaching  $45^\circ$  at altitudes around 5000 m in the granitoids of the Pangong Metamorphic Complex. These planes are associated with a stretching lineation plunging gently SSE and a crenulation lineation plunging gently NW. Best fit great circle through the C planes reveal a common axis of rotation parallel to the stretching lineation at 163/30 (open square). Shear indicators (Figure 9) indicate consistently an oblique shear sense composed of thrusting to the NNW and dextral motion.

asymmetric phenocrysts. Despite this close relationship no overprinting relationships could be determined. Shear sense in pelitic and psammitic rocks could not be determined unambiguously, in contrast to their very clear kinematic indicators elsewhere.

## 5. Metamorphism

[26] Rocks of the Karakoram Metamorphic Complex generally have amphibolite facies mineral assemblages, most evident in mafic units which consist of hornblende, plagioclase, biotite, quartz, and garnet. Finely recrystallized plagioclase grains exhibit  $120^\circ$  dihedral angles typical of amphibolite facies metamorphism. Within the pegmatitic leucogranite, quartz and plagioclase show recrystallization textures typical of temperatures exceeding  $>400^\circ\text{C}$  [Passchier and Trouw, 1998, p. 49] and with myrmekite alteration on the margins of large feldspar phenocrysts indicative of upper greenschist to amphibolite facies conditions [Vernon, 2004, p. 253].

[27] The lack of evidence for partial melting in muscovite-bearing schists and psammites indicates that temperatures remained below that of muscovite dehydration-melting in the presence of quartz and plagioclase. Quartz and plagioclase, which comprise the felsic groundmass of schists and psammites, also show a number of microstructures indicative of low- to medium-grade deformation. These include patchy to sweeping undulose extinction, tapering and bent deformation twins in plagioclase, rare deformation lamellae in quartz, and dynamic recrystallization through both bulging and subgrain rotation recrystallization.

[28] Greenschist facies retrogression of amphibolite facies rocks of the Karakoram Metamorphic Complex is represented by chlorite-actinolite-calcite schists  $\pm$  pyrite  $\pm$  magnetite. In places, retrogression is limited to rims around quartz veins in amphibolites. In other places, retrogression is pervasive and greenschist facies minerals are sheared dextrally (Figure 11). These features taken together are indicative of cooling from amphibolite to greenschist facies conditions during dextral shearing.

[29] In contrast to the Karakoram Metamorphic Complex, rocks of the Pangong Metamorphic Complex underwent anatexis by influx of water-rich fluids contemporaneous with shearing and folding that produced bodies of leucogranites-leucotonalites at a range of scales [Weinberg and Mark, 2008]. Deformation continued as the system cooled into subsolidus amphibolite facies conditions as revealed by sheared anatectic leucogranites [Weinberg *et al.*, 2009]. No evidence for greenschist facies retrogression has been documented.

[30] We used  $^{40}\text{Ar}/^{39}\text{Ar}$  geochronology to constrain differences in the timing of cooling between the Karakoram and Pangong metamorphic complexes. The samples analyzed consisted of three amphibole separates and one biotite separate from two different samples. Sample PNG19 ( $33^\circ59'51.8''\text{N}$ ,  $78^\circ21'42.5''\text{E}$ ) is from an amphibolite layer in the Karakoram Metamorphic Complex, northeast of the Pangong Strand, and sample TNG45mm ( $33^\circ58'12.5''\text{N}$ ,  $78^\circ22'41.6''\text{E}$ ) is from an anatectic hornblende-biotite leucogranite from the Pangong Metamorphic Complex. Both samples had no evidence of greenschist facies overprinting (sample locations in Figure 2).

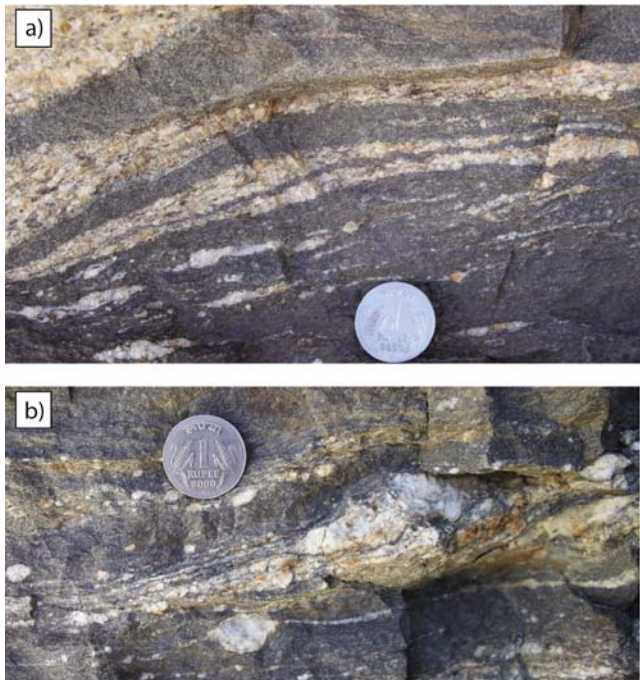


**Figure 9.** Two examples of thrusting with a dextral component (top to the right in photograph) in migmatitic rocks of the Pangong Metamorphic Complex in the Pangong Range (33°59'11.0"N, 78°18'47.2"E) SW of Chagar Tso in Figure 3. Shear sense is indicated by porphyroblast stair-stepping tails and C-S fabric. Field of view is vertical, nearly parallel to the stretching lineation and perpendicular to shear plane C (lineation trending 185/33 on a C plane trending 135/45 SW; Figure 8b).

[31] Figure 12 shows  $^{40}\text{Ar}/^{39}\text{Ar}$  step heating results for biotite and hornblende. Closure temperatures of argon are assumed to be  $\sim 500^\circ\text{C}$  for hornblende [e.g., Baldwin *et al.*, 1990] and  $\sim 300^\circ\text{C}$  for biotite [e.g., Harrison *et al.*, 1985], with an uncertainty of  $\pm 50^\circ\text{C}$  on both closure temperatures, encompassing variation expected due to compositional and dimensional effects on diffusion parameters [Renne *et al.*, 1993]. For results, refer to Tables 1 and 2.

[32] Biotite from sample TNG45mm yielded a disturbed spectrum, but with a reasonably concordant average age of  $10.57 \pm 0.26$  Ma ( $2\sigma$ ) (Figure 12a). The discordance in the age spectrum could possibly be the result of either different sized grains used for the analysis, Ar loss, or alteration around the grain margins. Of five hornblende aliquots from the same sample which underwent laser step heating (Table 2), some yielded consistent apparent age plateaus, though across all the analyses the ages were reasonably concordant, indicating timing of cooling through  $500^\circ\text{C}$  around  $13.34 \pm 0.14$  Ma ( $2\sigma$ ) (Figure 12b and Table 2).

[33] From the two hornblende aliquots from PNG19 from the Karakoram Metamorphic Complex (33°59'51.8"N, 78°21'42.5"E), one yielded a plateau age of  $22.73 \pm 0.74$  Ma ( $2\sigma$ ) (Figure 12c), encompassing 52.8% of the  $^{39}\text{Ar}$ , with a second sample showing an average age of  $22.5 \pm 0.9$  Ma.

All of the hornblende spectra show a very high initial age, decreasing sharply across the spectra toward the plateau age with increasing percentage of cumulative  $^{39}\text{Ar}$  released. This initial older age is possibly the result of degassing of fluid inclusions within the hornblende grains affecting the results of the initial heating steps. These results indicate differential cooling and presumably differential exhumation between the two metamorphic complexes. The Karakoram Metamorphic Complex cooled through  $500^\circ\text{C}$  around 22 Ma,  $\sim 9$  Myr before the Pangong Metamorphic Complex.

## 6. Discussion

### 6.1. Modern Trace of the Pangong Strand of the Karakoram Shear Zone

[34] The Karakoram Shear Zone has been previously defined as the  $\sim 7$ – $8$  km wide region between the Pangong and Tangtse strands [e.g., Searle *et al.*, 1998]. The Tangtse Strand marks a sharp boundary between sheared rocks of the Pangong Metamorphic Complex and weakly deformed rocks of the Ladakh Batholith. Narrowly defined, the Pangong Strand is marked by the lineament defined by the Muglib Valley, and geologically by the contact between the Pangong and Karakoram metamorphic complexes (Figures 3a and 3b). However, in the Pangong Strand mylonitic rocks form a much wider zone extending north of the lineament into the Karakoram Range for at least another 2 km. This implies that the northern boundary of the Karakoram Shear Zone has not yet been determined in this area, and that the shear zone is at least 10 km wide and includes rocks of the Karakoram Metamorphic Complex.

[35] The narrowly defined Pangong Strand marking the boundary between the two metamorphic complexes (Figure 3a), is a significant geological boundary, separating metasedimentary sequences of different metamorphic grades and is relatively easy to follow in the field and in satellite images (Figure 3a). Two contact areas between these metamorphic complexes were investigated here, one on the NW end of the area in Figure 3a, the other in the valley SW of Chagar Tso. In both areas, the contact is marked by a change from marbles and schists of the Karakoram Metamorphic Complex, to anatectic rocks of the Pangong Metamorphic Complex lacking marbles (Figure 9). Southwest of Chagar Tso, away from the contact and into the Pangong Range, migmatitic metasedimentary rocks give way to a relatively homogeneous, protomylonitic granodiorite body, part of the Muglib Pluton [Weinberg *et al.*, 2009]. No evidence of brittle faulting was found at either contact.

[36] A number of features indicative of recent movement along the fault have been mapped in the Muglib Valley, including offset debris flow levees and offset lateral moraines [Brown *et al.*, 2002], and a clay-bearing fault gauge zone overprinting ductile deformation [Rutter *et al.*, 2007] (locations in Figure 2). Despite this evidence, we mapped rock layers continuously through the area, suggesting that significant brittle displacement is either parallel to layering or has taken place away from the area covered by Figure 3b.

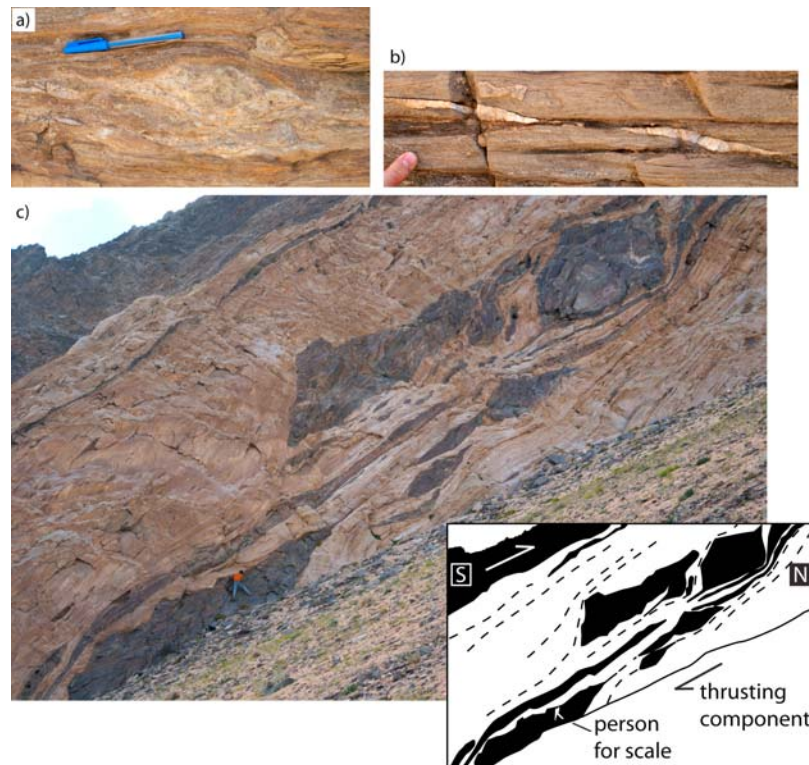


**Figure 10.** (a and b) Sinistral shear sense in metasedimentary rocks in outcrops immediately west of the northern tip of the Pangong Lake, looking parallel to lineation and perpendicular to foliation trending  $\sim 100^\circ$  (east is to the left). Figure 10a shows sigmoidal disrupted quartz veins. Figure 10b shows sinistral slip on plane separating sigmoidal segments of a quartz vein. (c) Stretched lozenges of amphibolite within strongly sheared marble (looking west from  $33^\circ 58' 3.0''\text{N}$ ,  $78^\circ 24' 04.8''\text{E}$ ) close to Figure 10a. Amphibolite lozenge asymmetry indicates a thrusting component of shearing to the north within a dominantly sinistral shear zone where lineation plunges gently ESE toward the viewer.

## 6.2. Metamorphism, Cooling, and Deformation

[37] Mesozoic platform sedimentary rocks present in the Chang-Chenmo Range located  $\sim 40$  km to northwest of the Karakoram Shear Zone in the Pangong Tso area, indicates that this region is not as deeply exhumed as the high-grade metamorphic rocks from within the Pangong Range [Dunlap *et al.*, 1998] which originated from depths of  $> 20$  km [Rolland and Pêcher, 2001]. It has been argued that exhumation of the Pangong Metamorphic Complex by movement on the Karakoram Shear Zone started after the end of magmatism [Dunlap *et al.*, 1998; Phillips *et al.*, 2004]. This was based on the impression that the shear zone cuts across the leucogranites which allowed the youngest age for leucogranites to be used as an upper bound to shear initiation. However, Weinberg and Mark [2008] have demonstrated the contemporaneity between anatexis, formation of leucogranites, and shearing, and suggested that shearing may have triggered anatexis through providing a permeable pathway for influx of water released from dehydrating metamorphic rocks. Thus, initiation of the shear zone may have preceded the oldest leucogranite dated at circa 20 Ma [Searle *et al.*, 1998; see also Valli *et al.*, 2007].

[38] The U-Pb age obtained from zircons in leucogranite samples of the Pangong Metamorphic Complex are interpreted to represent the timing of migmatization of the exposed sequence. This interpretation is based on field



**Figure 11.** Sigmoidal actinolite aggregates in a chlorite-calcite-rich matrix. C-S-C' fabrics and asymmetry of aggregates are indicative of dextral shear sense ( $33^\circ 59' 27.6''\text{N}$ ,  $78^\circ 20' 17.1''\text{E}$ ).

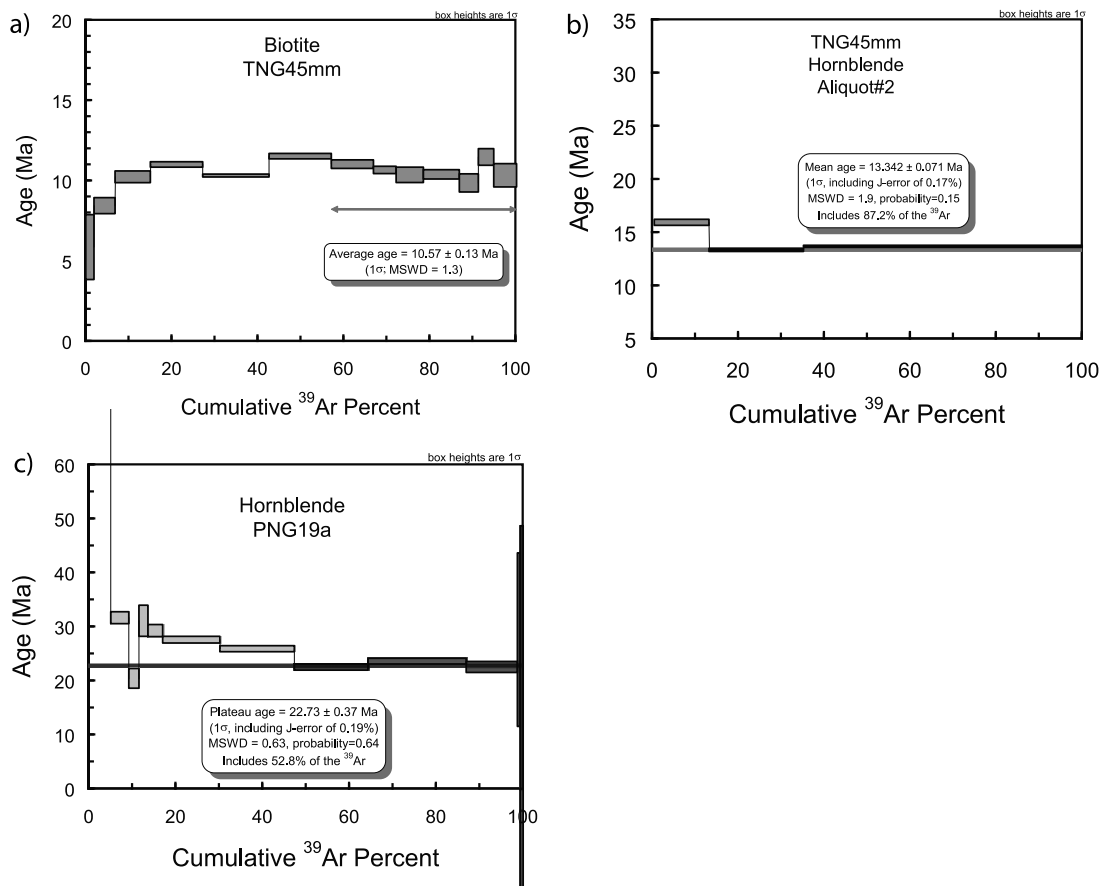


**Figure 12.** The  $^{40}\text{Ar}/^{39}\text{Ar}$  age spectra for (a) biotite and (b) hornblende from sample TNG45mm from the Pangong Metamorphic Complex and (c) hornblende from PNG19 from the Karakoram Metamorphic Complex. Sample locations shown in Figure 2. Full data for all aliquots are given in Tables 1 and 2. Note that in Figure 12a, no plateau age was defined; instead, we report an average age for the higher temperature steps marked by the horizontal arrow, and results in Figure 12b are from laser step-heating experiments.

relations that show the physical and chemical link between a network of leucosomes in the anatexitic source with leucogranite dykes and irregular sheets that feed into stocks and plutons [Reichardt *et al.*, 2010; Weinberg and Mark, 2008; Weinberg *et al.*, 2009]. If this is so, the Complex must have cooled across the leucogranite solidus of  $\sim 700^\circ\text{C}$  some time between 18 and 15 Ma, inferred to mark the time of peak magmatism [Phillips *et al.*, 2004; Ravikant *et al.*, 2009; Reichardt *et al.*, 2010; Searle *et al.*, 1998]. This was followed by cooling through the  $\sim 500^\circ\text{C}$  isotherm at around 13.5 Ma, based on three argon cooling age samples: (1) the one presented here, (2) the  $13.8 \pm 0.1$  Ma from hornblende sample 212 from within the Tangtse gorge between Tangtse and Muglib by Dunlap *et al.* [1998], and (3) the  $13.6 \pm 0.1$  Ma from hornblende sample L441 by Rolland *et al.* [2009].

[39] The  $300^\circ\text{C}$  isotherm was crossed sometime between circa 10.8 Ma (here) and  $9.7 \pm 0.1$  Ma (biotite samples 135 and 135A from within the Pangong Strand close to the village of Muglib of Dunlap *et al.* [1998]). Taken together this data suggest average cooling rates between  $50^\circ\text{C}$  and  $80^\circ\text{C}/\text{Myr}$ , from  $\sim 700^\circ\text{C}$  to  $300^\circ\text{C}$ . Lack of greenschist

facies retrogression rocks of the Pangong Metamorphic Complex suggest that most of its deformation took place during the early part of the cooling history from anatexis to lower amphibolite facies.

[40] The Karakoram Metamorphic Complex adjacent to the Pangong Strand, in contrast, never reached anatexis and the few analyses available suggests it cooled through  $\sim 500^\circ\text{C}$  isotherm much earlier, at around 22 Ma (sample PNG19), and then through  $\sim 300^\circ\text{C}$  of  $10.8 \pm 0.1$  Ma (muscovite sample 130 from a mylonitic marble of close to the Pangong Strand at Muglib of Dunlap *et al.* [1998]), roughly contemporaneous with the Pangong Metamorphic Complex. Sheared amphibolite facies rocks overprinted by sheared greenschist facies rocks suggest continuous deformation through cooling. Similar arguments were made by Rolland *et al.* [2009], who further pointed out the steep geothermal gradient of the Pangong Range of  $50^\circ\text{C}/\text{km}$  at 10 km depth. They argued that this could be a combined result of shear heating and extra heat advected by mantle-derived intrusions. We note that rapid exhumation of the Range could

**Table 1.** The <sup>40</sup>Ar/<sup>39</sup>Ar Furnace Step-Heating Analytical Results

| Temp (°C)   | Cumulative Percent <sup>39</sup> Ar | <sup>40</sup> Ar (×10 <sup>-13</sup> mol) | <sup>39</sup> Ar (×10 <sup>-14</sup> mol) | <sup>38</sup> Ar (×10 <sup>-16</sup> mol) | <sup>37</sup> Ar (×10 <sup>-16</sup> mol) | <sup>36</sup> Ar (×10 <sup>-16</sup> mol) | Ca/K             | <sup>40</sup> Ar* (%) | <sup>40</sup> Ar*/ <sup>39</sup> Ar | Age (Ma)    |
|---|-------------------------------------|---|---|---|---|---|------------------|-----------------------|-------------------------------------|-------------|
| <i>Sample TNG19(a) (Location 33°59'51.8"N, 78°21'42.5"E), J Value = 0.004786 ± 0.000009</i> |                                     |   |   |   |   |   |                  |                       |                                     |             |
| 800   | 2.48                                | 0.5602 ± 0.0012                           | 0.2058 ± 0.0010                           | 0.2292 ± 0.0274                           | 64.57 ± 0.4857                            | 1.0004 ± 0.0219                           | 5.4917 ± 0.0486  | 47.2                  | 12.86 ± 0.33                        | 107.7 ± 2.7 |
| 900   | 4.79                                | 0.8430 ± 0.0018                           | 0.1908 ± 0.0002                           | 0.2117 ± 0.0200                           | 141.01 ± 1.0016                           | 0.9290 ± 0.0156                           | 12.9314 ± 0.0930 | 67.4                  | 29.79 ± 0.26                        | 240.4 ± 2.0 |
| 1000  | 9.03                                | 0.4687 ± 0.0011                           | 0.3514 ± 0.0006                           | 0.2325 ± 0.0353                           | 275.77 ± 1.3960                           | 1.1498 ± 0.0157                           | 13.7348 ± 0.0737 | 27.5                  | 3.67 ± 0.14                         | 31.4 ± 1.2  |
| 1030  | 11.33                               | 0.2213 ± 0.0005                           | 0.1905 ± 0.0007                           | 0.1005 ± 0.0231                           | 137.99 ± 0.8127                           | 0.5982 ± 0.0138                           | 12.6739 ± 0.0876 | 20.1                  | 2.34 ± 0.22                         | 20.1 ± 1.8  |
| 1060  | 13.41                               | 0.2051 ± 0.0008                           | 0.1722 ± 0.0009                           | 0.0489 ± 0.0242                           | 148.72 ± 1.1302                           | 0.4844 ± 0.0194                           | 15.1164 ± 0.1370 | 30.2                  | 3.60 ± 0.34                         | 30.8 ± 2.9  |
| 1090  | 16.83                               | 0.2567 ± 0.0006                           | 0.2836 ± 0.0005                           | 0.1538 ± 0.0235                           | 469.17 ± 2.2164                           | 0.5443 ± 0.0125                           | 28.9525 ± 0.1447 | 37.3                  | 3.38 ± 0.13                         | 29.0 ± 1.1  |
| 1120  | 30.03                               | 0.5887 ± 0.0013                           | 1.0941 ± 0.0016                           | 0.5357 ± 0.0904                           | 2189.46 ± 9.1472                          | 0.8103 ± 0.0281                           | 35.0189 ± 0.1549 | 59.3                  | 3.19 ± 0.08                         | 27.4 ± 0.7  |
| 1150  | 47.19                               | 0.6784 ± 0.0014                           | 1.4212 ± 0.0017                           | 0.6576 ± 0.1191                           | 2920.99 ± 12.6391                         | 0.8566 ± 0.0302                           | 35.9676 ± 0.1615 | 62.7                  | 2.99 ± 0.06                         | 25.7 ± 0.5  |
| 1200  | 64.16                               | 0.6688 ± 0.0014                           | 1.4065 ± 0.0019                           | 0.6997 ± 0.1152                           | 2768.68 ± 11.5932                         | 1.0309 ± 0.0315                           | 34.4476 ± 0.1515 | 54.4                  | 2.59 ± 0.07                         | 22.2 ± 0.6  |
| 1250  | 86.91                               | 1.1678 ± 0.0043                           | 1.8844 ± 0.0044                           | 1.1755 ± 0.1547                           | 3777.52 ± 16.7599                         | 2.2149 ± 0.0390                           | 35.0811 ± 0.1762 | 44.0                  | 2.72 ± 0.07                         | 23.4 ± 0.6  |
| 1300  | 98.70                               | 0.7407 ± 0.0018                           | 0.9774 ± 0.0011                           | 0.6613 ± 0.0851                           | 1882.74 ± 7.7042                          | 1.6500 ± 0.0384                           | 33.7109 ± 0.1428 | 34.2                  | 2.59 ± 0.12                         | 22.2 ± 1.0  |
| 1350  | 99.44                               | 0.9065 ± 0.0054                           | 0.6067 ± 0.0006                           | 0.6226 ± 0.0193                           | 110.84 ± 0.9172                           | 3.0021 ± 0.0343                           | 31.9363 ± 0.4183 | 2.1                   | 3.19 ± 1.89                         | 27.3 ± 16.1 |
| 1450  | 100.00                              | 1.8404 ± 0.0042                           | 0.0467 ± 0.0002                           | 1.3067 ± 0.0182                           | 81.01 ± 0.5022                            | 6.2021 ± 0.0616                           | 30.3669 ± 0.2270 | 0.4                   | 1.65 ± 4.00                         | 14.2 ± 34.3 |
| <i>Sample TNG19(b) (Location 33°59'51.8"N, 78°21'42.5"E), J Value = 0.004786 ± 0.000009</i> |                                     |   |   |   |   |   |                  |                       |                                     |             |
| 800   | 4.07                                | 0.4855 ± 0.0011                           | 0.2586 ± 0.0008                           | 0.2407 ± 0.0308                           | 49.03 ± 0.8211                            | 1.0444 ± 0.0311                           | 3.3179 ± 0.0565  | 36.4                  | 6.84 ± 0.36                         | 58.1 ± 3.0  |
| 900   | 8.04                                | 0.8046 ± 0.0017                           | 0.2524 ± 0.0009                           | 0.2134 ± 0.0208                           | 139.07 ± 0.9626                           | 1.0931 ± 0.0241                           | 9.6406 ± 0.0748  | 59.9                  | 19.08 ± 0.30                        | 157.6 ± 2.3 |
| 1000  | 15.61                               | 1.0176 ± 0.0023                           | 0.4815 ± 0.0013                           | 0.6786 ± 0.0472                           | 348.68 ± 1.4173                           | 3.0980 ± 0.0268                           | 12.6721 ± 0.0617 | 10.0                  | 2.12 ± 0.17                         | 18.2 ± 1.5  |
| 1090  | 27.67                               | 0.7053 ± 0.0016                           | 0.7667 ± 0.0012                           | 0.4786 ± 0.0645                           | 1281.16 ± 6.0043                          | 1.4906 ± 0.0273                           | 29.2423 ± 0.1441 | 37.6                  | 3.45 ± 0.11                         | 29.6 ± 0.9  |
| 1120  | 60.83                               | 1.0288 ± 0.0024                           | 2.1089 ± 0.0025                           | 0.9686 ± 0.1728                           | 4242.58 ± 17.4349                         | 1.4060 ± 0.0391                           | 35.2057 ± 0.1504 | 59.6                  | 2.91 ± 0.06                         | 24.9 ± 0.5  |
| 1150  | 63.81                               | 0.1751 ± 0.0004                           | 0.1891 ± 0.0004                           | 0.1341 ± 0.0256                           | 330.58 ± 1.5726                           | 0.4142 ± 0.0255                           | 30.5871 ± 0.1561 | 30.1                  | 2.79 ± 0.40                         | 23.9 ± 3.4  |
| 1180  | 68.31                               | 0.2339 ± 0.0008                           | 0.2864 ± 0.0009                           | 0.2483 ± 0.0276                           | 554.16 ± 2.8434                           | 0.5623 ± 0.0118                           | 33.8658 ± 0.2027 | 29.0                  | 2.37 ± 0.13                         | 20.3 ± 1.1  |
| 1220  | 78.85                               | 0.3939 ± 0.0009                           | 0.6700 ± 0.0016                           | 0.3684 ± 0.0543                           | 1350.96 ± 5.6358                          | 0.7901 ± 0.0234                           | 35.2839 ± 0.1684 | 40.7                  | 2.39 ± 0.10                         | 20.6 ± 0.9  |
| 1260  | 90.39                               | 0.3681 ± 0.0008                           | 0.7339 ± 0.0011                           | 0.4923 ± 0.0598                           | 1485.19 ± 6.5501                          | 0.5729 ± 0.0228                           | 35.4142 ± 0.1651 | 54.0                  | 2.71 ± 0.09                         | 23.2 ± 0.8  |
| 1300  | 97.35                               | 0.2194 ± 0.0005                           | 0.4427 ± 0.0012                           | 0.1701 ± 0.0395                           | 858.34 ± 4.2051                           | 0.3242 ± 0.0194                           | 33.9309 ± 0.1896 | 56.3                  | 2.79 ± 0.13                         | 24.0 ± 1.1  |
| 1450  | 100.00                              | 0.3339 ± 0.0010                           | 0.1685 ± 0.0007                           | 0.2324 ± 0.0296                           | 319.63 ± 1.4312                           | 0.9666 ± 0.0125                           | 33.2034 ± 0.2074 | 14.5                  | 2.86 ± 0.23                         | 24.6 ± 1.9  |
| <i>Sample TNG45(b) (Location 33°58'12.5"N, 78°22'41.6"E), J Value = 0.004789 ± 0.000008</i> |                                     |   |   |   |   |   |                  |                       |                                     |             |
| 600   | 1.90                                | 0.3251 ± 0.0007                           | 0.3043 ± 0.0011                           | 0.1845 ± 0.0305                           | 0.0085 ± 0.0004                           | 1.0320 ± 0.0243                           | 0.0005 ± 0.0000  | 6.2                   | 0.66 ± 0.24                         | 5.7 ± 2.0   |
| 650   | 6.81                                | 0.3663 ± 0.0008                           | 0.7866 ± 0.0009                           | 0.1200 ± 0.0659                           | 0.8174 ± 0.2911                           | 0.9825 ± 0.0153                           | 0.0182 ± 0.0065  | 20.7                  | 0.97 ± 0.06                         | 8.3 ± 0.5   |
| 700   | 15.00                               | 0.3588 ± 0.0008                           | 1.3101 ± 0.0017                           | 0.1129 ± 0.1074                           | 1.4354 ± 0.3840                           | 0.6928 ± 0.0187                           | 0.0192 ± 0.0051  | 42.9                  | 1.18 ± 0.04                         | 10.1 ± 0.4  |
| 750   | 27.13                               | 0.3700 ± 0.0008                           | 1.9433 ± 0.0018                           | 0.0627 ± 0.1586                           | 1.5865 ± 0.5284                           | 0.4189 ± 0.0133                           | 0.0143 ± 0.0048  | 66.5                  | 1.27 ± 0.02                         | 10.9 ± 0.2  |
| 800   | 42.48                               | 0.3757 ± 0.0008                           | 2.4572 ± 0.0017                           | 0.0569 ± 0.1994                           | 2.1972 ± 0.1760                           | 0.2865 ± 0.0091                           | 0.0156 ± 0.0013  | 77.4                  | 1.18 ± 0.01                         | 10.2 ± 0.1  |
| 850   | 57.00                               | 0.3391 ± 0.0008                           | 2.3244 ± 0.0017                           | 0.0004 ± 0.1887                           | 1.0281 ± 0.3937                           | 0.1038 ± 0.0157                           | 0.0077 ± 0.0030  | 90.9                  | 1.33 ± 0.02                         | 11.4 ± 0.2  |
| 900   | 66.82                               | 0.2407 ± 0.0007                           | 1.5720 ± 0.0033                           | 0.0004 ± 0.1302                           | 1.4970 ± 0.3170                           | 0.1396 ± 0.0163                           | 0.0167 ± 0.0035  | 82.8                  | 1.27 ± 0.03                         | 10.9 ± 0.3  |
| 950   | 72.08                               | 0.1443 ± 0.0004                           | 0.8431 ± 0.0010                           | 0.0319 ± 0.0706                           | 1.0962 ± 0.2814                           | 0.1382 ± 0.0076                           | 0.0228 ± 0.0058  | 71.7                  | 1.23 ± 0.03                         | 10.6 ± 0.2  |
| 1000  | 78.41                               | 0.1902 ± 0.0004                           | 1.0123 ± 0.0017                           | 0.0438 ± 0.0860                           | 1.7749 ± 0.5136                           | 0.2358 ± 0.0187                           | 0.0307 ± 0.0089  | 63.4                  | 1.19 ± 0.05                         | 10.3 ± 0.5  |
| 1050  | 86.73                               | 0.2466 ± 0.0008                           | 1.3321 ± 0.0032                           | 0.0426 ± 0.1083                           | 1.3906 ± 0.4524                           | 0.2965 ± 0.0152                           | 0.0183 ± 0.0059  | 64.5                  | 1.19 ± 0.03                         | 10.3 ± 0.3  |
| 1100  | 91.15                               | 0.1477 ± 0.0003                           | 0.7078 ± 0.0030                           | 0.0287 ± 0.0592                           | 1.6176 ± 0.2906                           | 0.2288 ± 0.0158                           | 0.0400 ± 0.0072  | 54.2                  | 1.13 ± 0.07                         | 9.7 ± 0.6   |
| 1150  | 94.73                               | 0.1162 ± 0.0004                           | 0.5740 ± 0.0016                           | 0.0025 ± 0.0491                           | 0.0085 ± 0.0079                           | 0.1365 ± 0.0118                           | 0.0003 ± 0.0002  | 65.3                  | 1.32 ± 0.06                         | 11.4 ± 0.5  |
| 1350  | 100.00                              | 0.2530 ± 0.0007                           | 0.8433 ± 0.0016                           | 0.0499 ± 0.0703                           | 6.3683 ± 0.2370                           | 0.5173 ± 0.0238                           | 0.1322 ± 0.0049  | 39.6                  | 1.19 ± 0.08                         | 10.2 ± 0.7  |



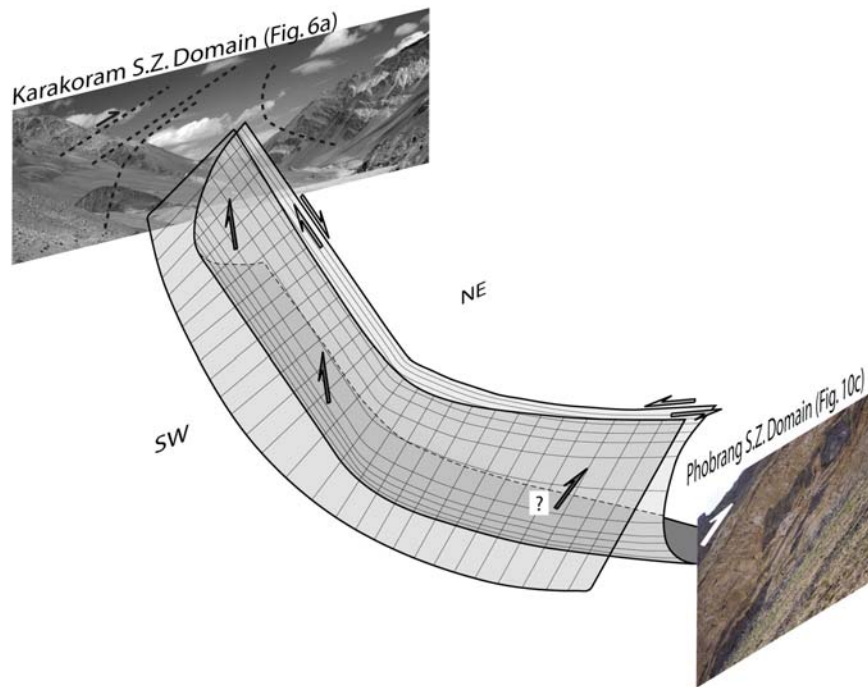


**Figure 13.** Diagrammatic 3-D representation of the thrust plane that places the Pangong Metamorphic Complex (PMC) over the folded Karakoram Metamorphic Complex (KMC), looking northward. The curved shape of the thrust is a result of sinistral movement on the late Phobrang Shear Zone.

lead to steep geothermal gradients without the need for extra heat sources.

[41] We postulate that deformation and cooling of the migmatitic rock sequence of the Pangong Metamorphic Complex mark its exhumation due to transpression on the Karakoram Shear Zone. Meanwhile, the Karakoram Metamorphic Complex was being underthrust and folded without having its amphibole cooling ages reset. At around 10 Ma there was no resolvable temperature difference between the two complexes, suggesting slow relative vertical movement between them. This could be due to (1) a change to dominant strike-slip movement or (2) amalgamation of the two complexes due to localization of shearing to a brittle fault outside the area. In summary, most of the relative exhumation recorded by the Pangong Metamorphic Complex took place during the 5 to 8 Myr period of rapid cooling between the end of anatexis and 10 Ma.

### 6.3. Large-Scale Fold

[42] Evidence from the area surrounding Chagar Tso (Figures 3a, 8b, 9, and 10) indicates that the Pangong Range was thrust obliquely toward the NNW on planes dipping moderately SW. We combine (1) dextral thrusting on moderately SW dipping planes on the Pangong Range, (2) the kilometric-scale, inclined-to-recumbent fold in the Muglib Valley and Karakoram Range (Figures 6 and 7), and (3) the relative exhumation of the two metamorphic complexes to suggest that these features record the oblique thrusting of the Pangong onto the Karakoram Metamorphic Complex by motion on the Karakoram Shear Zone, causing

drag folding of the lower-grade footwall sequence (Figure 13).

[43] The relative timing of dextral and sinistral movements on the Karakoram and Phobrang shear zones, respectively, remains undetermined. We infer that they are broadly contemporaneous because of similarities in shear textures and mineralogy indicative of similar metamorphic facies during dextral and sinistral shearing. Broad contemporaneity combined with strain partitioning explains the thrusting movement of the Pangong Metamorphic Complex over the Karakoram Metamorphic Complex and the change in horizontal motion from dextral to sinistral accompanying the bending in the regional trend (Figure 13).

[44] The kinematic evolution of the area is consistent with that resulting from analog experiments of indentation of a rigid block into a stratified lithosphere [Rosenberg *et al.*, 2007]. The experiments were run with orientations analogous to those in the Karakoram Shear Zone and shows that a rigid indenter pushing roughly northward on to weaker surroundings impose dextral transpression parallel to its NW–SE long side. This gives rise to a parallel region of folding and dextral shearing, equivalent to the Pangong Range. It also generates conjugate sinistral shear zones, approximately in the orientation and position of the Phobrang Shear Zone and the Longmu Tso–Gozha Tso fault system [see Rosenberg *et al.*, 2007, Figures 6a, 6d, and 7]. We postulate that the evolution of the area results from such an indentation, and that the then cool Ladakh Batholith [Dunlap *et al.*, 1998] could have acted as a rigid indenter as it lies immediately south of the Pangong Range.

[45] The structures documented here do not support Raterman *et al.*'s [2007] conclusion that the 27 km wide bend in the trend of the Karakoram Shear Zone around the Pangong Range results from transtension imposed by the triple junction with the sinistral Longmu Tso Fault, 40 km to the north of the area studied here. We confirm earlier conclusions [Weinberg *et al.*, 2000] that the bend is caused by transpression and splitting of the Karakoram Shear Zone into two strands, wrapping around the Pangong Range, allowing the exhumation of its high-grade metamorphic rocks.

## 7. Conclusions

[46] We conclude that dextral transpression imposed by a rigid indenter pushing to the north, possibly the Ladakh

Batholith, could explain (1) the exhumation of the Pangong Metamorphic Complex, (2) the large-scale drag folding of the Karakoram Metamorphic Complex underneath the thrust exhuming the Pangong Metamorphic Complex, and (3) the development of the sinistral system. The rocks mapped record intense and pervasive ductile deformation over wide zones in the form of shearing and folding, and rigid block conceptualization of continental crust deformation and kinematic analyses may yield misleading results if ductile deformation is neglected.

[47] **Acknowledgments.** We thank Geordie Mark and Henning Reichardt for discussions in the field. We thank also the Associate Editor, Hervé Leloup, and an anonymous reviewer for their thoughtful reviews which helped to improve this paper.

## References

- Baldwin, S. L., T. M. Harrison, and J. D. Fitzgerald (1990), Diffusion of  $^{40}\text{Ar}$  in metamorphic hornblende, *Contrib. Mineral. Petrol.*, **105**, 691–703, doi:10.1007/BF00306534.
- Bhutani, R., K. Pande, and N. Desai (2003), Age of the Karakoram fault activation:  $^{40}\text{Ar}/^{39}\text{Ar}$  geochronological study of Shyok suture zone in northern Ladakh, India, *Curr. Sci.*, **84**(11), 1454–1458.
- Brown, E. T., R. Bendick, D. L. Bourlès, V. Gaur, P. Molnar, G. M. Raisbeck, and F. Yiou (2002), Slip rates of the Karakoram fault, Ladakh, India, determined using cosmic ray exposure dating of debris flows and moraines, *J. Geophys. Res.*, **107**(B9), 2192, doi:10.1029/2000JB000100.
- Chevalier, M. L., F. J. Ryerson, P. Tapponnier, R. C. Finkel, J. Van der Woerd, H. B. Li, and Q. Liu (2005), Slip-rate measurements on the Karakoram Fault may imply secular variations in fault motion, *Science*, **307**(5708), 411–414, doi:10.1126/science.1105466.
- Dunlap, W. J., R. F. Weinberg, and M. P. Searle (1998), Karakoram fault zone rocks cool in two phases, *J. Geol. Soc. London*, **155**, 903–912, doi:10.1144/gsjgs.155.6.0903.
- Harrison, T. M., I. Duncan, and I. McDougall (1985), Diffusion of  $^{40}\text{Ar}$  in biotite: Temperature, pressure and compositional effects, *Geochim. Cosmochim. Acta*, **49**, 2461–2468, doi:10.1016/0016-7037(85)90246-7.
- Lacassin, R., *et al.* (2004a), Large-scale geometry, offset and kinematic evolution of the Karakoram Fault, Tibet, *Earth Planet. Sci. Lett.*, **219**(3–4), 255–269, doi:10.1016/S0012-821X(04)00006-8.
- Lacassin, R., *et al.* (2004b), Reply to comment on “Large-scale geometry, offset and kinematic evolution of the Karakoram fault, Tibet,” *Earth Planet. Sci. Lett.*, **229**(1–2), 159–163, doi:10.1016/j.epsl.2004.07.045.
- Murphy, M. A., and W. P. Burgess (2006), Geometry, kinematics, and landscape characteristics of an active transtension zone, Karakoram fault system, southwest Tibet, *J. Struct. Geol.*, **28**(2), 268–283, doi:10.1016/j.jsg.2005.10.009.
- Murphy, M. A., A. Yin, P. Kapp, T. M. Harrison, D. Lin, and J. H. Guo (2000), Southward propagation of the Karakoram fault system, southwest Tibet: Timing and magnitude of slip, *Geology*, **28**(5), 451–454, doi:10.1130/0091-7613(2000)28<451:SPOTKF>2.0.CO;2.
- Murphy, M. A., A. Yin, P. Kapp, T. M. Harrison, C. E. Manning, F. J. Ryerson, L. Ding, and J. H. Guo (2002), Structural evolution of the Gurla Mandhata detachment system, southwest Tibet: Implications for the eastward extent of the Karakoram fault system, *Geol. Soc. Am. Bull.*, **114**(4), 428–447, doi:10.1130/0016-7606(2002)114<0428:SEOTGM>2.0.CO;2.
- Passchier, C. W., and R. A. J. Trouw (1998), *Microtectonics*, 289 pp., Springer, Berlin.
- Peltzer, G., and P. Tapponnier (1988), Formation and evolution of strike-slip faults, rifts, and basins during the India-Asia collision: An experimental approach, *J. Geophys. Res.*, **93**, 15,085–15,117, doi:10.1029/JB093iB12p15085.
- Phillips, D., and J. W. Harris (2008), Provenance studies from  $^{40}\text{Ar}/^{39}\text{Ar}$  dating of mineral inclusions in diamonds: Methodological tests on the Orapa kimberlite, Botswana, *Earth Planet. Sci. Lett.*, **274**, 169–178, doi:10.1016/j.epsl.2008.07.019.
- Phillips, G., C. J. L. Wilson, D. Phillips, and S. Szczepanski (2007), Thermochronological ( $^{40}\text{Ar}/^{39}\text{Ar}$ ) evidence for Early Palaeozoic basin inversion within the southern Prince Charles Mountains, East Antarctica: Implications for East Gondwana, *J. Geol. Soc.*, **164**, 771–784, doi:10.1144/0016-76492006-073.
- Phillips, R. J., and M. P. Searle (2007), Macrostructural and microstructural architecture of the Karakoram Fault: Relationship between magmatism and strike-slip faulting, *Tectonics*, **26**, TC3017, doi:10.1029/2006TC001946.
- Phillips, R. J., R. R. Parrish, and M. P. Searle (2004), Age constraints on ductile deformation and long-term slip rates along the Karakoram fault zone, Ladakh, *Earth Planet. Sci. Lett.*, **226**(3–4), 305–319, doi:10.1016/j.epsl.2004.07.037.
- Raterman, N. S., E. Cowgill, and D. Lin (2007), Variable structural style along the Karakoram Fault explained using triple-junction analysis of intersecting faults, *Geosphere*, **3**(2), 71–85, doi:10.1130/GES00067.1.
- Ravikant, V. (2006), Utility of Rb–Sr geochronology in constraining Miocene and Cretaceous events in the eastern Karakoram, Ladakh, India, *J. Asian Earth Sci.*, **27**, 534–543, doi:10.1016/j.jseae.2005.05.007.
- Ravikant, V., F. Y. Wu, and W. Q. Ji (2009), Zircon U–Pb and Hf isotopic constraints on petrogenesis of the Cretaceous–Tertiary granites in eastern Karakoram and Ladakh, India, *Lithos*, **110**, 153–166.
- Reichardt, H., R. F. Weinberg, U. B. Andersson, and M. C. Fanning (2010), Hybridization of granitic magmas in the source: The origin of the Karakoram Batholith, Ladakh, NW India, *Lithos*, **116**, 249–272.
- Renne, P. R., O. T. Tobisch, and J. B. Saleeby (1993), Thermochronologic record of pluton emplacement, deformation, and exhumation at Courtright shear zone, central Sierra Nevada, *Calif. Geol.*, **21**, 331–334.
- Renne, P. R., C. C. Swisher, A. L. Deino, D. B. Karner, T. L. Owens, and D. J. DePaolo (1998), Intercalibration of standards, absolute ages and uncertainties in  $^{40}\text{Ar}/^{39}\text{Ar}$  dating, *Chem. Geol.*, **145**, 117–152, doi:10.1016/S0009-2541(97)00159-9.
- Rolland, Y., and A. Pêcher (2001), The Pangong granulites of the Karakoram Fault (western Tibet): Vertical extrusion within a lithosphere-scale fault?, *C. R. Acad. Sci., Ser. II*, **6**, 363–370.
- Rolland, Y., G. Mahéo, A. Pêcher, and I. M. Villa (2009), Syn-kinematic emplacement of the Pangong metamorphic and magmatic complex along the Karakoram Fault (N Ladakh), *J. Asian Earth Sci.*, **34**(1), 10–25, doi:10.1016/j.jseae.2008.03.009.
- Rosenberg, C. L., J.-P. Brun, F. Cagnard, and D. Gapais (2007), Oblique indentation in the Eastern Alps: Insights from laboratory experiments, *Tectonics*, **26**, TC2003, doi:10.1029/2006TC001960.
- Rutter, E. H., D. R. Faulkner, K. H. Brodie, R. J. Phillips, and M. P. Searle (2007), Rock deformation processes in the Karakoram fault zone, eastern Karakoram, Ladakh, NW India, *J. Struct. Geol.*, **29**(8), 1315–1326, doi:10.1016/j.jsg.2007.05.001.
- Searle, M. P. (1996), Geological evidence against large-scale pre-Holocene offsets along the Karakoram Fault: Implications for the limited extrusion of the Tibetan Plateau, *Tectonics*, **15**(1), 171–186, doi:10.1029/95TC01693.
- Searle, M. P., and R. J. Phillips (2004), A comment on “Large-scale geometry, offset, and kinematic evolution of the Karakoram Fault, Tibet” by R. Lacassin *et al.*, *Earth Planet. Sci. Lett.*, **229**(1–2), 155–158, doi:10.1016/j.epsl.2004.07.044.
- Searle, M. P., and R. J. Phillips (2007), Relationships between right-lateral shear along the Karakoram Fault and metamorphism, magmatism, exhumation and uplift: Evidence from the K2–Gasherbrum–Pangong ranges, north Pakistan and Ladakh, *J. Geol. Soc.*, **164**, 439–450, doi:10.1144/0016-76492006-072.
- Searle, M. P., R. F. Weinberg, and W. J. Dunlap (1998), Transpressional tectonics along the Karakoram fault zone, northern Ladakh: Constraints on Tibetan extrusion, in *Continental Transpressional and Transpressional Tectonics*, edited by R. E. Holdsworth *et al.*, *Geol. Soc. Spec. Publ.*, **135**, 307–326, doi:10.1144/GSL.SP.1998.135.01.20.
- Upadhyay, R., J. Rai, and A. K. Sinha (2005), New record of Bathonian–Callovian calcareous nannofossils in the eastern Karakoram block: A possible clue to understanding the dextral offset along the Karakoram Fault, *Terra Nova*, **17**(2), 149–157, doi:10.1111/j.1365-3121.2005.00602.x.
- Valli, F., N. Arnaud, P. H. Leloup, E. R. Sobel, G. Mahéo, R. Lacassin, S. Guillot, H. Li, P. Tapponnier, and Z. Xu (2007), Twenty million years of continuous deformation along the Karakoram Fault, western Tibet: A thermochronological analysis, *Tectonics*, **26**, TC4004, doi:10.1029/2005TC001913.
- Valli, F., *et al.* (2008), New U–Th/Pb constraints on timing of shearing and long-term slip-rate on the Karakoram Fault, *Tectonics*, **27**, TC5007, doi:10.1029/2007TC002184.

- Vernon, R. H. (2004), *A Practical Guide to Rock Microstructures*, 594 pp., Cambridge Univ. Press, Cambridge, U. K.
- Weinberg, R. F., and W. J. Dunlap (2000), Growth and deformation of the Ladakh Batholith, northwest Himalayas: Implications for timing of continental collision and origin of calc-alkaline batholiths, *J. Geol.*, *108*, 303–320, doi:10.1086/314405.
- Weinberg, R. F., and G. Mark (2008), Magma migration, folding, and disaggregation of migmatites in the Karakoram Shear Zone, Ladakh, NW India, *Geol. Soc. Am. Bull.*, *120*, 994–1009, doi:10.1130/B26227.1.
- Weinberg, R. F., W. J. Dunlap, and M. Whitehouse (2000), New field, structural and geochronological data from the Shyok and Nubra valleys, northern Ladakh: Linking Kohistan to Tibet, in *Tectonics of the Nanga Parbat Syntaxis and the Western Himalaya*, edited by T. P. J. Khan et al., *Geol. Soc. Spec. Publ.*, *170*, 253–275, doi:10.1144/GSL.SP.2000.170.01.14.
- Weinberg, R. F., G. Mark, and H. Reichardt (2009), Magma ponding in the Karakoram Shear Zone, Ladakh, NW India, *Geol. Soc. Am. Bull.*, *121*, 278–285.
- Wright, T. J., B. Parsons, P. C. England, and E. J. Fielding (2004), InSAR observations of low slip rates on the major faults of western Tibet, *Science*, *305*(5681), 236–239, doi:10.1126/science.1096388.

---

M. R. McCarthy and R. F. Weinberg, School of Geosciences, Monash University, Clayton, Vic 3800, Australia. (roberto.weinberg@sci.monash.edu.au)